*J. Plasma Physics* (2008), *vol.* 74, *part* 3, *pp.* 301–318. © 2008 Cambridge University Press 
doi:10.1017/S0022377808007095 Printed in the United Kingdom

# Test kinetic modelling of collisionless perpendicular shocks

F. MACKAY, R. MARCHAND, K. KABIN and J.Y. LU

Department of Physics, University of Alberta, Edmonton Alberta, T6G 2G7 Canada
(rmarchan@ualberta.ca)

(Received 6 February 2007 and in revised form 21 May 2007, first published online 13 February 2008)

**Abstract.** Test kinetic simulation results are presented for perpendicular collisionless shocks in magnetized plasmas that are representative of the Earth's bow shock. In this approach, particle kinetics are described by tracing particle trajectories in prescribed electromagnetic fields obtained in the MHD approximation, and applying Liouville's theorem. This provides a first-order description of particle dynamics in complex systems, given approximate fields obtained with a low-level description of the plasma. The method also provides a useful consistency check in assessing the validity of approximate solutions such as those obtained in the ideal MHD approximation. Compared with the more familiar test particle approach, in which trajectories of randomly injected particles are followed in time, the present approach has the advantage of being numerically more efficient, and producing results without statistical errors.

## 1. Introduction

In addition to being interesting from a theoretical standpoint, collisionless shock waves are encountered in a variety of laboratory and astrophysical phenomena. For example, in near Earth and planetary space environments magnetospheres are separated from the incoming solar wind by a transition region called the bow shock. Within the Galaxy, our own Solar System is also contained in a plasma environment delimited by a termination shock. Shocks are also ubiquitous in many transient astrophysical phenomena such as solar flares, supernovae, collisions between black holes, etc. It is also likely that collisionless shocks were at play in the early epochs of our Universe, when they may have been responsible for the creation of the very energetic cosmic rays still observed today (Jones and Ellison 1991). Shocks have been proposed as a mechanism capable of generating very high energy cosmic radiation. For example, under certain conditions, charged particles may effectively be picked up, surf on strong shock fronts and be energized to relativistic energies (Zank et al. 1996; Lee et al. 1996; Lever et al. 2001; Zank et al. 2006). In addition to affecting particle energies, shocks are also known to lead to anisotropy and phase bunching in the distribution of particle momentum. As a consequence, shock regions are generally accompanied by free energy responsible for plasma wave instabilities and turbulence. These phenomena, in turn, will influence wave activity and, more generally, plasma transport properties in shocked regions.

Over the years, the study of shock waves has attracted considerable attention among the modelling community. The most advanced studies now make use of

https://doi.org/10.1017/S0022377808007095 Published online by Cambridge University Press

multi-dimensional hybrid (Burgess and Scholer 2007), or fully kinetic self-consistent calculations (Othmer et al. 2000; Haruki et al. 2006). At the same time many interesting problems are still being studied with approximate fluid models. In these approaches, shocks are described in terms of mass, momentum and energy conservation equations. When complemented with Maxwell's equations, these conservation laws yield the familiar Rankine–Hugoniot conditions for plane shocks (Kantrowitz and Petschek 1966). Modified forms of the Rankine–Hugoniot conditions have been proposed to account, for example, for the effect of multiple fluids (Sanderson and Uhrig 1978), pressure anisotropy (Chao et al. 1995; Karimabadi et al. 1995), finite heat flux (Lyu and Kan 1986) and the presence of spatial modulations and waves on either side of the interface (Lin and Lee 1994). These modifications were motivated by discrepancies between observed actual shocks and predictions from ideal MHD theory. While useful in better reconciling theory and observation, these modified models remain fundamentally macroscopic, and they are not designed to study or assess kinetic aspects of particle transport across shocks, which are only accessible from a suitable calculation of the particle distribution function. Such effects include, for example, particle energization associated with surfing (Lee et al. 1996; Lever et al. 2001) the formation of populations of foreshock particles (Gosling et al. 1978; Thomas and Winske 1990), phase bunching (McKean 1995; Astudillo et al. 1996; Meziane et al. 2001), phase space anisotropy (Lembege and Dawson 1987; Thomas 1989); shock front instabilities and turbulence (Tanaka et al. 1983; Schwartz et al. 1996; Burgess and Scholer 2007), and their effect on phase space isotropization (McKean 1996).

In this article we use a test-particle-like approach, hereafter referred to as the test-kinetic approach, to provide an approximate description of particle kinetics in a shock, without carrying out a fully self-consistent kinetic calculation. This method relies on an approximate calculation of the electromagnetic fields with a low-level (i.e. macroscopic) model, followed by backward particle trajectory integrations, and the use of Liouville's theorem. The resulting distribution function is of course approximate. In particular, the lack of self-consistency results in moments of the distribution function not agreeing exactly with the fluid results used to calculate the approximate fields in the first place. Despite its lack of consistency, this approach has been used in earlier studies, for example, to estimate distribution functions of particles in the magnetotail (Jaeger and Speiser 1974) and their sources (Ashour-Abdalla et al. 1999) or as an interpretative tool in magnetic reconnection experiments using experimentally measured fields (Egedal et al. 2004). We believe that, while not fully self-consistent, the approach considered here is useful because it does provide a first estimation of particle kinetic effects in cases where a good approximation of the fields is available. It also provides a useful check in assessing the consistency of field solutions obtained in the macroscopic approximation. Thus, in cases where moments of the approximate distribution function would agree with the mass, momentum and energy densities obtained with a fluid model, the validity of the fluid approximation would be verified. In cases where there would be substantial discrepancies, on the other hand, we would know that the fluid model is missing some important physics associated with particle kinetics. We note that Liouville's theorem and backward particle integration may be used to provide a fully self-consistent calculation of the distribution function. Such a calculation, however, would require iterations between the calculated particle distribution in phase space and the fields (Hozumi 1977).

https://doi.org/10.1017/S0022377808007095 Published online by Cambridge University Press

The remainder of this article is organized as follows. In Sec. 2 we explain the test-kinetic method in the context of a plane shock wave obtained with the standard Rankine–Hugoniot conditions. Section 3 presents example results of the test-kinetic approach, in which similarities and differences with the underlying macroscopic approach are identified. In Sec. 4, results are presented for a variety of shock conditions, and scaling relations are presented for pressure anisotropy and phase bunching for various shock conditions. Finally, Sec. 5 contains a summary of our results and some concluding remarks.

## 2. The test-kinetic approach

A useful way to introduce the test-kinetic approach is to draw a parallel with the more familiar test-particle approach. In both cases, approximate fields obtained from a low-level (non-kinetic) model are used to compute particle trajectories in order to study bulk properties of the medium. These approaches are not fully self-consistent and, as such, they can only provide an approximate description of plasma particle dynamics. The quality of the approximate solutions depends, of course, on the accuracy of the approximate fields used to calculate particle trajectories. Ultimately, if one were to apply these methods with the exact fields, including fine spacial and temporal dependences, then an exact description of particle dynamics would result. In addition to providing approximate descriptions of particle kinetics, both methods are useful in providing a consistency check of fluid simulation results. For example, if the test-particle approach is used to calculate density and average velocity profiles that correspond to a given approximate MHD solution, and if the resulting profiles are in good agreement with those of the MHD solution, then those solutions can be deemed to be satisfactory. If, on the other hand, the moments calculated with the test-particle approximation (the particle density and the current density for example) differed significantly from the corresponding variables obtained from the MHD solution, then one would conclude that the latter approximation misses important aspects of the physics that requires a consistent treatment of particle kinetics.

The test-particle and test-kinetic approaches differ in two important ways. Firstly, while the former approach relies on an integration of particle trajectories forward in time, the test-kinetic approach performs trajectory integrations backward in time and it relies on Liouville's theorem to calculate the particle distribution function at various positions in phase space. Secondly, the test-particle approach may be used to study properties of single particle trajectories (Moore et al. 2000; Delcourt 2002; Takeuchi 2005) or to calculate macroscopic averages from the calculations of large numbers ($\sim 10^9$) of particles injected randomly in space (Richard et al. 2002; Delcourt et al. 2003; Moore et al. 2005; Delcourt et al. 2006). This typically results in appreciable statistical errors, particularly in multi-dimensional problems, or when considering high-order moments of the distribution function. The test-kinetic approach, on the other hand, makes use of particle trajectories with initial conditions on a given grid in momentum space. This is then used to calculate the distribution of particles at precise times and positions in space. The distribution function at those positions must then be interpolated from its discretization on a grid. The resulting errors are interpolation or truncation errors. The method, however, is free from statistical errors. In what follows, we limit our discussion to the test-kinetic approach.

https://doi.org/10.1017/S0022377808007095 Published online by Cambridge University Press

Let us consider a collisionless plasma described by the Vlasov equation

$$\frac{\partial f}{\partial t} + \frac{d\mathbf{r}}{dt} \cdot \nabla f + \frac{d\mathbf{p}}{dt} \cdot \frac{\partial f}{\partial \mathbf{p}} = 0, \tag{2.1}$$

where

$$\frac{d\mathbf{r}}{dt} = \frac{\partial H}{\partial \mathbf{p}} \tag{2.2}$$

and

$$\frac{d\mathbf{p}}{dt} = -\frac{\partial H}{\partial \mathbf{r}}. \tag{2.3}$$

In these equations, $f$ is the phase space density distribution function, $\mathbf{r}$ and $\mathbf{p}$ are canonical coordinate and momentum vectors, respectively, and $H$ is the Hamiltonian. For simplicity, the particle distribution function $f$ will be assumed to be independent of time, although the same formalism would equally apply to problems with a time dependence. Equation (2.1) is seen to have the same form as Liouville's equation for the phase space density of a system of particles. As with Liouville's theorem, the physical interpretation of the Vlasov equation is that the distribution function $f$ is constant along a particle trajectory in phase space. Making use of that property, it is then possible to calculate $f(\mathbf{r}, \mathbf{p})$ at an arbitrary position $\mathbf{r}$ and momentum $\mathbf{p}$ by simply tracing a particle trajectory from that position in phase space, back in time, until it reaches a region where the distribution function $f$ is known. Such a region will be referred to in what follows as a source region. Thus, if the particle reaches a source region, say, at position $\mathbf{r}_0$ with momentum $\mathbf{p}_0$, it follows from Liouville's theorem that

$$f(\mathbf{r}, \mathbf{p}) = f(\mathbf{r}_0, \mathbf{p}_0). \tag{2.4}$$

In applying (2.4), it is important to account for the fact that some particles may cross the shock interface more than once. For that reason, the trajectory integration leading to point $(\mathbf{r}_0, \mathbf{p}_0)$ must not be stopped as soon as the particle reaches the upstream region. In this problem, the integration is stopped only after the particle has spent a complete gyro-period exclusively in the upstream region. If the procedure described above is applied to the vertices of a grid in momentum space, at various points in configuration space, it yields a detailed discretization of the distribution function $f$ on that momentum grid at arbitrary positions in space. This discretization, in turn, can be interpolated to produce an approximate representation of $f$ in phase space. Various moments of $f$ may then be calculated from this approximation, and directly compared with results obtained from the underlying MHD (or, more generally, fluid) approximation. As mentioned previously, the resulting moments may suffer from interpolation errors in momentum space, but they are free from statistical error. On a practical note, the structure of $f$ in momentum space may be somewhat irregular and, in general, difficult to predict. Yet, $f$ must be well resolved in order to reduce interpolation errors. We therefore use an adaptive mesh in momentum space, based on an octree decomposition of an initially coarse and uniform rectangular grid (Frey and George 1999). These ideas will be applied to a simple example in the following section. Before proceeding with results, however, it is worth making the following general remarks.

https://doi.org/10.1017/S0022377808007095 Published online by Cambridge University Press

### *2.1. Maximum value of f*

If a system consists of a single source region in which the distribution function $f$ is uniform (independent of position), then the maximum value of $f$ is the same everywhere in space. This can be understood from the very nature of the test-kinetic approach. Because use is made of the fact that $f$ is constant along a particle trajectory, the value of $f$ at an arbitrary point $\mathbf{r}$ in space must be traceable (by backward integration in time) to a corresponding point $\mathbf{r}_0$ in the input region. It is clear, then, that the maximum value of $f$ at $\mathbf{r}$ must be the same as that at $\mathbf{r}_0$. Examples of systems with a single and uniform input region include idealized plane shocks, or a magnetosphere subject to steady and uniform solar wind conditions, when ionospheric outflow is negligible. Note that it is possible for the maximum value of $f$ to be less than the maximum value in the source region if the position considered is inaccessible to particles in the source region, for which $f$ is maximum. Conversely, under some conditions, it may not be possible to trace particle trajectories back to the input region for some positions and momenta. The corresponding values of $f$ will then vanish, as these points in phase space will not be accessible to any particle from the input region.

### *2.2. Symplectic integration*

The method used here to calculate $f$ relies on the distribution function remaining constant along particle trajectories. This, in turn, is equivalent to the phase space density being constant along particle trajectories. It is therefore essential to use an integration technique when calculating particle trajectories that preserves these important properties. Such integration techniques are known as symplectic. Several symplectic schemes have been proposed in the literature. For example, when the Hamiltonian is separable, that is, when it can be written as

$$H(\mathbf{r}, \mathbf{p}) = T(\mathbf{r}) + V(\mathbf{p}), \tag{2.5}$$

explicit high-order symplectic integration schemes can be constructed (Candy and Rozmus 1990). More generally, high-order symplectic integrations require implicit methods (Sanz-Serna 1988; Suris 1989; Yoshida 1993; Shimada and Yoshida 1996; Stuchi 2002). In this study, we use a fourth-order implicit scheme (also referred to as the implicit Runge–Kutta scheme) as described in a recent article (Mackay et al. 2006). It should be noted that explicit Runge–Kutta integration schemes are generally not symplectic. Therefore, even if such schemes can be constructed with high-order accuracy and adaptive time steps, they should be avoided or used with caution in test-particle or test-kinetic approaches.

## 3. Plane perpendicular shock

Let us consider a plane shock in a magnetized collisionless plasma. For convenience, we formulate the problem in the shock frame of reference, that is, in a frame in which the shock is stationary. Without loss of generality, we assume that the plasma flow velocity $v$ is perpendicular to the shock interface. Shocks with flows that have a tangential component can always be reduced to this situation with a suitable Galilean transformation. Finally, for simplicity, we limit our attention to a perpendicular shock, that is, one for which the magnetic field $B$ is perpendicular to the normal to the shock interface. To be specific, referring to the usual $x, y, z$ Cartesian system of coordinates, we assume that the magnetic field is along $z$, the

https://doi.org/10.1017/S0022377808007095 Published online by Cambridge University Press

fluid velocity is along the $+y$ direction and the shock front is in the $xz$ plane. Under these assumptions, the shock conditions are completely determined by conservation laws for mass, momentum and energy, as well as the stationary form of Faraday's law ($\nabla \times \mathbf{E} = 0$), where, in the ideal MHD approximation, $\mathbf{E} = -\mathbf{v} \times \mathbf{B}$. When the differential forms of these equations are integrated across the assumed shock discontinuity, one obtains the familiar Rankine–Hugoniot conditions:

$$[v\rho] = 0, \tag{3.1}$$

$$[vB] = 0, \tag{3.2}$$

$$\left[\rho v^2 + p + \frac{B^2}{2\mu_0}\right] = 0, \tag{3.3}$$

$$\left[\rho v^3 + \frac{\gamma}{\gamma - 1} pv + \frac{B^2 v}{\mu_0}\right] = 0. \tag{3.4}$$

In these equations, brackets indicate differences between downstream and upstream quantities at the interface, $\rho$ is the plasma mass density, $\mu_0$ is the magnetic permeability of vacuum and $\gamma$ is the ratio of the specific heat at constant pressure to that at constant volume, $\gamma = C_p/C_v$. These equations can readily be solved analytically to yield

$$v_2 = \zeta v_1, \tag{3.5}$$

$$B_2 = \frac{1}{\zeta} B_1, \tag{3.6}$$

$$p_2 = p_1 + (1 - \zeta)\rho_1 v_1^2 - \frac{1 - \zeta^2}{\zeta^2} \frac{B_1^2}{2\mu_0}, \tag{3.7}$$

where $\zeta$ is the ratio of the upstream to downstream density,

$$\zeta = \frac{\rho_1}{\rho_2}. \tag{3.8}$$

In the following, it will be sufficient to limit our attention to the special case $\gamma = 2$, for which

$$\zeta = \frac{\rho_1 v_1^2 + 4(p_1 + B_1^2/2\mu_0)}{3\rho_1 v_1^2}. \tag{3.9}$$

A more general solution valid for arbitrary values of $\gamma$ has been derived, for example, by Kabin (2000). The condition for this solution to be valid is that it corresponds to a compressional shock ($\zeta < 1$), for which specific entropy increases across the shock. Equations (3.5)–(3.9) constitute the solution to the perpendicular plane shock problem in the MHD approximation. We recall that in our analytic solution physical parameters are assumed to be constant on both sides of the shock front, and that they are mathematically discontinuous at the shock interface. In order to avoid numerical difficulties at the shock interface, however, the discontinuity is approximated by a narrow but smooth transition over a layer of thickness $\delta$. In the following section we present numerical results obtained from the application of Liouville's theorem and a high-order symplectic integration of particle trajectories. In this approach, the equations of motion are expressed in terms of the scalar and vector potentials $\phi$ and $\mathbf{A}$ instead of the electric and magnetic fields $\mathbf{E}$ and $\mathbf{B}$, where

https://doi.org/10.1017/S0022377808007095 Published online by Cambridge University Press

the electric field is obtained in the ideal MHD approximation as

$$\mathbf{E}_i = -\mathbf{v}_i \times \mathbf{B}_i, \tag{3.10}$$

where the subscript $i$ stands for 1 or 2 to denote variables on either side of the shock front. In our geometry, $\mathbf{E}$ is seen to be directed along the $-\hat{x}$ axis, with its $x$ component given by $E_i = -v_i B_i$. Thus, the corresponding four-vector potential is written as

$$\phi = \frac{(\phi_2 - \phi_1)}{2} \tanh\left(\frac{y}{\delta}\right) + \frac{\phi_1 + \phi_2}{2} \tag{3.11}$$

and

$$\mathbf{A} = \frac{\mathbf{A}_2 - \mathbf{A}_1}{2} \tanh\left(\frac{y}{\delta}\right) + \frac{\mathbf{A}_1 + \mathbf{A}_2}{2}, \tag{3.12}$$

where

$$\phi_i = x v_i B_i \tag{3.13}$$

and

$$\mathbf{A}_i = (0, x B_i, 0). \tag{3.14}$$

In the following calculations we use a value for $\delta$ that is small enough for the transition to appear as nearly discontinuous on a macroscopic scale, but large enough to avoid discontinuities in trajectory integrations. In practice, using one-tenth of a thermal gyroradius in the upstream region,

$$\delta = \frac{1}{10}\sqrt{\frac{2T_1}{m}}\frac{m}{qB_1} \tag{3.15}$$

gives satisfactory results. In (3.15) $T_1$ is the upstream plasma temperature and $m$ represents the proton mass (corresponding to a hydrogen plasma). In what follows, both ions and electrons are assumed to have the same temperature.

## 4. Numerical results

In this section we use the test-kinetic formalism to calculate the ion distribution functions in simple test problems. Our results reveal some aspects of kinetic properties of collisionless shocks. They are also compared against those of the ideal MHD approximation to provide a consistency check of the solution obtained from applying the Rankine–Hugoniot conditions.

With the conditions stated in the previous section (ideal MHD, $\gamma = 2$ and the assumption of a stationary plane perpendicular shock), the solution to the shock problem as determined by the Rankine–Hugoniot conditions is found to be a function of the two dimensionless parameters $\tilde{M}$ and $\beta$, where

$$\tilde{M}^2 = v_1 \Big/ \left(\gamma \frac{p_1 + B_1^2/2\mu_0}{\rho_1}\right) \tag{4.1}$$

and

$$\beta = \frac{p_1}{B_1^2/(2\mu_0)}. \tag{4.2}$$

This is useful, as it reduces the problem initially involving three variables $\rho_1$, $B_1$ and $v_1$ to one involving only these two independent variables. Before looking at solutions over a range of parameters $\tilde{M}$ and $\beta$, it is informative to consider the

https://doi.org/10.1017/S0022377808007095 Published online by Cambridge University Press

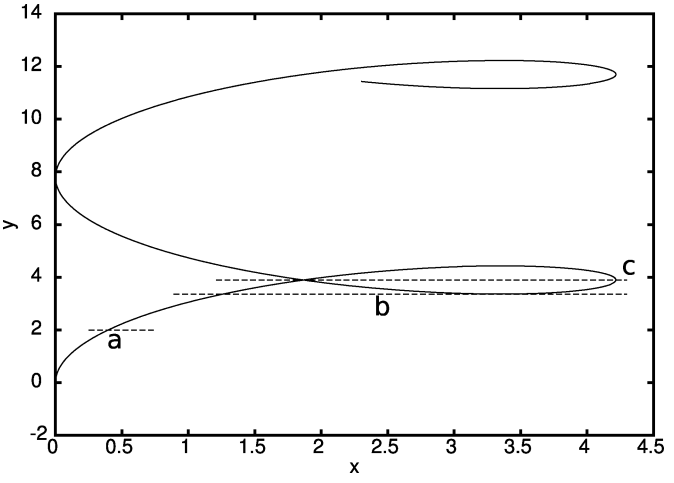



**Figure 1.** Trajectory of a particle initially drifting in a straight line at velocity $\mathbf{v}_1 = \mathbf{E}_1 \times \mathbf{B}_1/B_1^2$ in the upstream region, corresponding to the maximum of $f$ there. As it enters the shocked region, the particle has a perpendicular velocity that is larger than the local $\mathbf{E}_2 \times \mathbf{B}_2$ velocity. As a result, its trajectory becomes a cycloid.

solution obtained in one particular case, and understand in what ways it agrees with or differs from the approximate ideal MHD solution. For that purpose, we choose a shock corresponding to upstream conditions with a particle density $n_1 = 10^6$ m$^{-3}$, temperature $T_1 = 15.65$ eV, magnetic field $B_1 = 4.01 \times 10^{-9}$ T and velocity $v_1 = 4.95 \times 10^5$ m s$^{-1}$. These correspond to typical solar wind parameters 1 AU from the sun. Assuming equal ion and electron densities and temperatures, these parameters correspond to $\tilde{M} = 4.24$ and $\beta = 0.783$.

As stated above, the use of the test-kinetic approach relies on the knowledge of the distribution function $f$ in the input region. For consistency with the ideal MHD model, the particle distribution function in the upstream region is assumed to be a drifting Maxwellian with uniform density and temperature, that is,

$$f(\mathbf{r}, \mathbf{p}) = n\left(\frac{m}{2\pi T}\right)^{3/2} \exp\left(\frac{(\mathbf{p} - m\mathbf{v}_1)^2}{2mT}\right), \tag{4.3}$$

where $m$ is the proton mass. We note that, upstream of the shock interface, particles for which the distribution is maximum are $\mathbf{E} \times \mathbf{B}$ drifting in a straight line in the $+y$ direction.

### *4.1. The distribution function*

Some basic features of the distribution function can be understood in terms of a single particle trajectory for a particle travelling with a momentum for which the distribution function is maximum. With the assumptions made above, such a particle $\mathbf{E} \times \mathbf{B}$ drifts in a straight line in the upstream region. It enters the shocked region with velocity $v_1 > v_2$, $v_2$ being the $\mathbf{E} \times \mathbf{B}$ drift velocity in the shocked region. The particle then follows a cycloid trajectory as illustrated in Fig. 1. Making use of the fact that the distribution function $f$ remains constant along particle trajectories, it is possible to understand the morphology of the distribution function in momentum space at different penetrations into the shocked region. For example, it is clear that $f$ will have a single maximum in momentum space at position (a),

https://doi.org/10.1017/S0022377808007095 Published online by Cambridge University Press

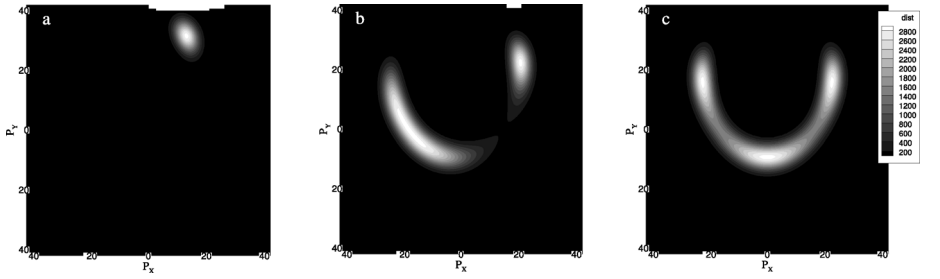



**Figure 2.** Sample distribution functions corresponding to positions a, b and c in Fig. 1.

at which both $p_x$ and $p_y$ will be positive (the particle for which $f$ is maximum is moving upward and to the right). At position (b), however, there are two maxima; one corresponding to the particle moving to the left ($p_x < 0$ and $p_y = 0$) and another one corresponding to the particle moving upward to the right ($p_x$ and $p_y$ both positive). Similarly, at position (c), there are three maxima in $f$, corresponding to the particle moving up to the right ($p_x > 0$, $p_y > 0$), down ($p_x = 0$ and $p_y < 0$) and up to the left ($p_x < 0$ and $p_y > 0$). These features are seen in Fig. 2, where the distribution function is plotted in terms of $p_x, p_y$, in the $p_z = 0$ plane, at the three positions corresponding to a, b and c in Fig. 1. In this figure, and in the following ones, all coordinates are normalized relative to the thermal gyroradius in the upstream region,

$$\rho_{\mathrm{th1}} = \sqrt{\frac{2T_1}{m}}\frac{m}{eB} = \sqrt{\frac{p_1}{\rho_1}}\frac{m}{eB}, \tag{4.4}$$

where use is made of the assumption $p = p_{\mathrm{e}} + p_{\mathrm{i}}$ with $p_{\mathrm{e}} = p_{\mathrm{i}}$. We note that the periodicity in the trajectory shown in Fig. 1 implies that the maximum in $f$ will also exhibit periodic features as a function of the penetration distance into the shocked region. The associated length period $\lambda$ is related to the gyroperiod and the drift velocity in that region through

$$\lambda = v_2 \frac{2\pi m}{eB_2}. \tag{4.5}$$

In this example, the drift velocity on either side of the shock front is several times the plasma thermal velocity. As a result, essentially all the particles in the distribution cross the interface only once and, starting at $y = 0$, the distribution function itself and its moments are nearly periodic in $y$, with length period $\lambda$. It should be noted that if, in contrast, a significant fraction of particles in the distribution crossed the interface more than once, a phenomenon known as 'shock surfing', then the solution would effectively become periodic only past a certain distance into the shocked region.

Figure 3 shows the trajectory of an energetic particle (500 eV—many times the thermal energy) with a phase such that it crosses the shock front more than once. That particle is seen to cross the interface three times before it definitely enters the shocked region. In that process, the particle drifts along the shock interface (surfs), to the left. This drift is opposite to that experienced by the bulk of the particles, which cross the shock front only once and have their guiding centre displaced to the right. Considering that, in our geometry, the electric field is pointing in the negative $x$ direction, it follows that energetic surfing particles get further energized by the

https://doi.org/10.1017/S0022377808007095 Published online by Cambridge University Press

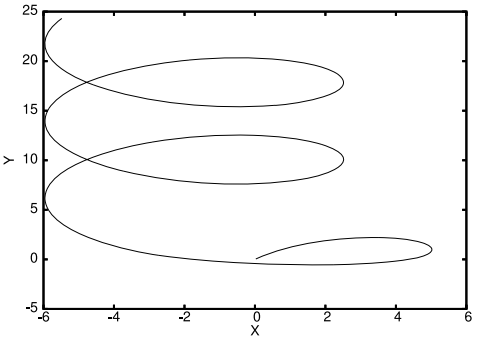



**Figure 3.** Example trajectory of a 500 eV particle crossing the shock front at an angle such that it is reflected back to the preshock region, then drifts in the direction of the electric field and crosses the front again. As a result, this 'surfing' particle gains kinetic energy.

shock, while low-energy (thermal) particles tend to loose energy to the electric field. Referring to Fig. 3, it can be understood that, if a significant fraction of the particles (up to three or four times thermal) cross the interface more than once, then the solution in the shocked region will effectively be periodic only beyond a distance $d$ into the shocked region, where $d$ is the deepest penetration distance of one of these particles before its final crossing of the shock interface. In the example shown in Fig. 3, periodicity in $y$ involving particles with thermal energy 500 eV or less would be in the range $3 \lesssim y$.

### *4.2. Consistency of the test-kinetic solution*

A connection between the solution of the test-kinetic problem and the solution of the Rankine–Hugoniot conditions is readily made by calculating moments of the distribution function and comparing them with the corresponding macroscopic variables. The simplest physical quantity to consider is the particle density, which is obtained from the zeroth moment of $f$. A comparison between the density calculated in the ideal MHD approximation and in the test-kinetic approach is given in Fig. 4. In this figure, the MHD density profile has a step-like discontinuity at the interface. As for the zeroth moment of $f$, consistent with the previous discussion on the periodic nature of the distribution function in the shocked region, the zeroth moment of $f$ is seen to be periodic, with periodicity $\lambda$. When averaged spatially over the period $\lambda$, however, the test-kinetic density is seen to agree very well with the Rankine–Hugoniot prediction. In this problem, the agreement between the MHD and spatially averaged densities is found to be within approximately 0.1%. The small discrepancy is due to discretization errors in the representation of $f$ on a grid. In that sense, the test-kinetic approach is seen to provide some of the features of kinetic collisionless shocks, in particular periodic features in the distribution function and in its moments, while being consistent with the underlying approximate MHD solution.

Another comparison of interest concerns the thermal pressure. While pressure appears as a contribution in the Rankine–Hugoniot conditions, it does not appear by itself as a standalone condition. It is therefore of interest to see to what extent the test-kinetic pressure compares with that obtained in the fluid approximation. The first difference to note is that the thermal pressure assumed in the fluid equations is a scalar. That is, the MHD model assumes that the thermal pressure

https://doi.org/10.1017/S0022377808007095 Published online by Cambridge University Press

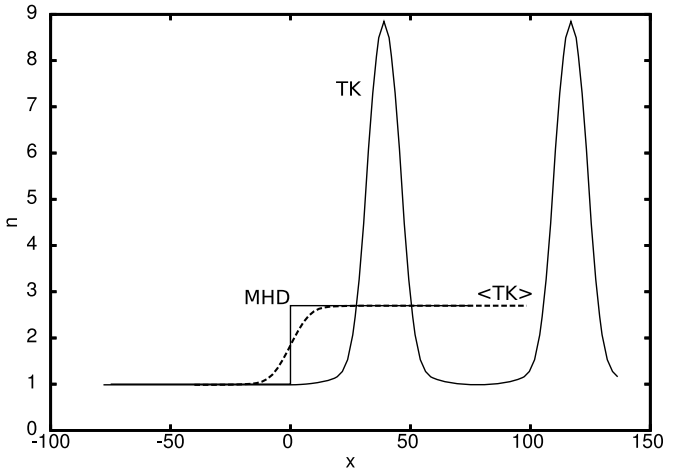



**Figure 4.** Comparison between the ideal MHD density profile (discontinuous step function) and that calculated in the test-kinetic approximation (TK). When averaged over one length period (dashed), the test-kinetic density is in excellent agreement with that obtained from solving the Rankine–Hugoniot conditions.

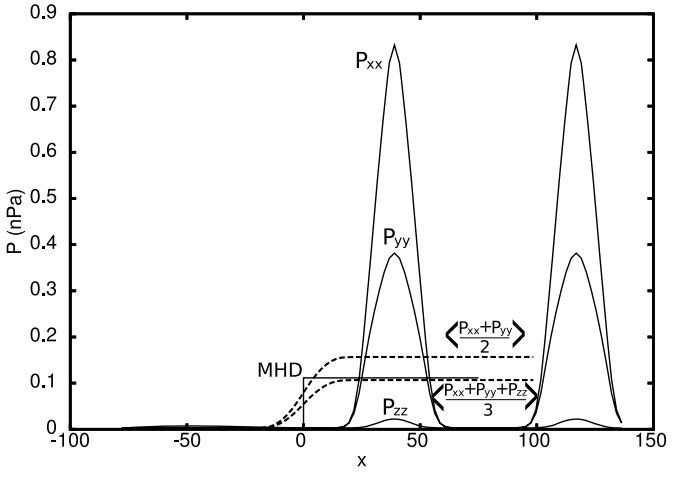



**Figure 5.** Comparison between the ideal MHD pressure profile (discontinuous step function) and diagonal components of the thermal pressure tensor calculated in the test-kinetic approximation. When averaged over one length period (dashed), the total test-kinetic pressure agrees approximately with that obtained from solving the Rankine–Hugoniot conditions.

tensor is diagonal and isotropic on either side of the shock front. The thermal stress tensor calculated in the test-kinetic model, on the other hand, has non-zero off-diagonal components, and its diagonal components are not all equal. This is shown in Fig. 5, in which the ideal MHD scalar pressure is compared with the three diagonal components of the thermal stress tensor and various averages thereof. The diagonal components of the stress tensor exhibit similar periodic structures as the density in Fig. 4. It is apparent from Fig. 5 that the pressure tensor is anisotropic,

https://doi.org/10.1017/S0022377808007095 Published online by Cambridge University Press

as the maximum values of the three components of $P$ are seen to be significantly different. As with density, it is interesting to see that the scalar (MHD) pressure in the shocked region agrees well with the spatial average of the mean of the three diagonal components of $P$. This agreement, however, is only approximate, and it is a function of the parameters $\tilde{M}$ and $\beta$. For larger values of $\tilde{M}$ ($\tilde{M} \gtrsim 2$), the thermal pressure inferred from the Rankine–Hugoniot conditions tends to agree better with the spatial average of the mean of the two perpendicular diagonal components of the pressure tensor. For lower Mach numbers ($\tilde{M} < 2$), however, the Rankine–Hugoniot conditions tend to produce a pressure in the shocked region, which falls between the spatial averages of $(P_{xx} + P_{yy} + P_{zz})/3$ and $(P_{xx} + P_{yy})/2$. The discrepancies found between the ideal MHD pressure and those obtained in the test-kinetic approximation are more significant than those found for the density. The small differences observed with the density are associated with numerical truncation errors. The differences found with the pressure, on the other hand, are associated with the lack of consistency of the test-kinetic approach. Indeed, while the pressure, the magnetic and electric field (albeit indirectly through $\mathbf{E} = \mathbf{v} \times \mathbf{B}$) contribute in the Rankine–Hugoniot conditions, the explicit expression of these conditions relies on the use of Maxwell's equations, together with a number of mathematical identities. Thus, for example, in a fully self-consistent calculation, the contribution $\rho\mathbf{E} + \mathbf{J} \times \mathbf{V}$ in the momentum conservation equation may be rewritten in terms of a divergence of the Maxwell stress tensor $\partial_j T_{ji}$, where

$$T_{ji} = \epsilon_0 \left( E_j E_i - \frac{\delta_{ij}}{2} E^2 \right) + \frac{1}{\mu_0} \left( B_j B_i - \frac{\delta_{ij}}{2} B^2 \right). \tag{4.6}$$

As noted above, however, due to the lack of consistency in the test-particle approach, the current and charge densities obtained in that approach do not satisfy Maxwell's equations, when considered with the approximate prescribed electromagnetic fields. It is therefore not possible to satisfy the types of equivalence implied in (4.6); whence the discrepancy between the two solutions.

This lack of consistency is further illustrated by directly considering Ampère's law. In the stationary shock problem assumed here, the discontinuity in the magnetic field must be associated with a surface current density,

$$\mathbf{J} = \frac{B_2 - B_1}{\mu_0} \delta(y) \hat{x}. \tag{4.7}$$

The $x$ component of the $y$-integrated current density in (4.7) and that resulting from the test-kinetic approximation are shown in Fig. 6. The integrated current density calculated in the test-kinetic approximation is seen to have periodic features, with the same periodicity $\lambda$ as other moments calculated in that approximation. The important point to note in this figure is that the spatial average (over $\lambda$) of the depth integrated current as calculated in the test-kinetic approximation only accounts for approximately 50% of the $y$-integrated surface current inferred from applying Ampère's equation to the solution of the Rankine–Hugoniot conditions. The missing contribution to the current cannot be attributed to electrons as, in this model, the contribution to the current due to a species is proportional to the particle mass. The electron contribution to the current density is therefore negligible compared to that of ions. The violation of a relation as fundamental as Ampère's law may be disturbing at first. This is understandable, however, as it results from the fact that, even though Ampère's law and other Maxwell equations are involved implicitly in

https://doi.org/10.1017/S0022377808007095 Published online by Cambridge University Press

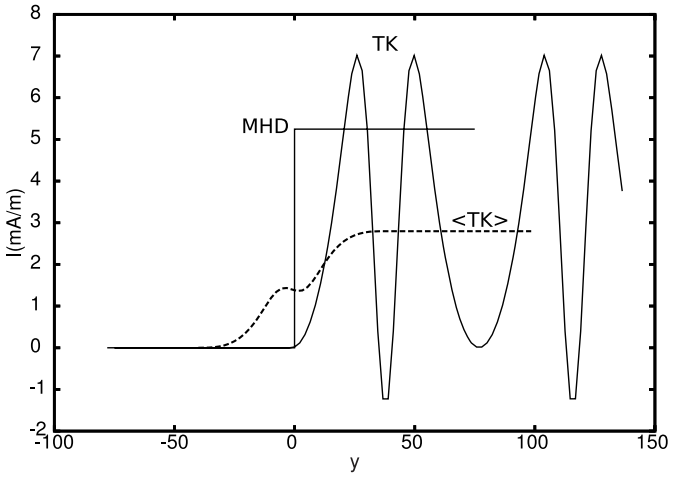



**Figure 6.** Comparison between the depth integrated current density obtained from the Rankine–Hugoniot conditions (MHD) and the test-kinetic model (TK, periodic solid curve). The spatial average of the integrated test-kinetic current (dashed curve) only accounts for approximately 50% of the expected current.

the formulation of the Rankine–Hugoniot conditions, they do not appear explicitly in the matching conditions. Furthermore, the Rankine–Hugoniot conditions are formulated in terms of macroscopic quantities ($\rho$, $v$ and $p$) in which the connection between these quantities and the fields is much simpler than that provided by the test-kinetic approach. It is for these reasons, because of the incompleteness of the underlying equations and of the lack of consistency, that the test-particle approach leads to results that differ from what one might expect from the initial approximate (ideal MHD) solution.

### *4.3. Anisotropy, phase bunching and current consistency*

Despite the inconsistencies noted above, it is of interest to explore the dependence of the solution in terms of the two dimensionless parameters $\beta$ and $\tilde{M}$. This is of interest in view of the continued reference to the Rankine–Hugoniot conditions in the literature (Dasgupta et al. 2006; Zank et al. 2006; Yong et al. 2006). The characterization of the inconsistency between the test-kinetic approach and the Rankine–Hugoniot conditions also provides a useful assessment of the validity of the latter approximation of collisionless shocks.

To start with, let us consider aspects of the simulation results that are intrinsically kinetic in nature. To be specific, let us consider pressure anisotropy, $P_\perp/P$ and phase bunching. Phase bunching, or velocity non-gyrotropy, refers to the occurrence of non-uniform distributions of particles in gyrophase at a given point in space. A precise characterization of phase bunching would require a detailed knowledge of the distribution function in phase space or, equivalently, of many of its moments. For convenience, we limit our assessment to the ratio of the two perpendicular components of the pressure stress tensor, $P_{xx}/P_{yy}$. In calculating this ratio, each component is first averaged spatially over $\lambda$. This then provides a unique ratio which does not depend on the position $y$ in the shocked region. An estimate of consistency, on the other hand, is provided by comparing the test-kinetic spatially

https://doi.org/10.1017/S0022377808007095 Published online by Cambridge University Press

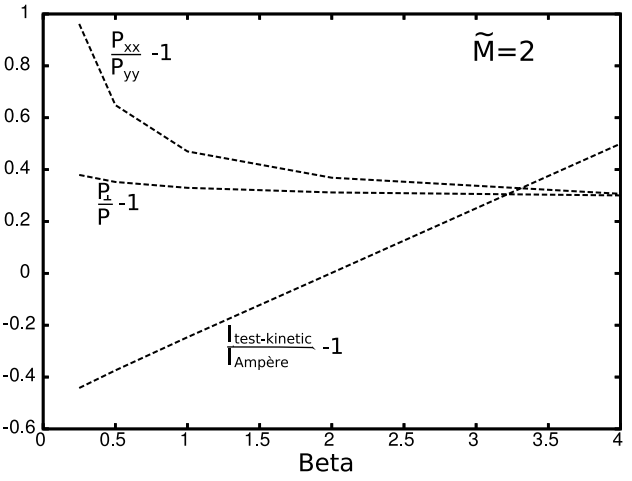



**Figure 7.** Scaling of the spatially averaged pressure anisotropy $P_\perp/P$, $P_{xx}/P_{yy}$ and discrepancy in the depth integrated current density as a function of $\beta$. All ratios are calculated from spatially averaged quantities so as to be uniquely defined in the shocked region. In all cases, the shock Mach number is equal to 2.

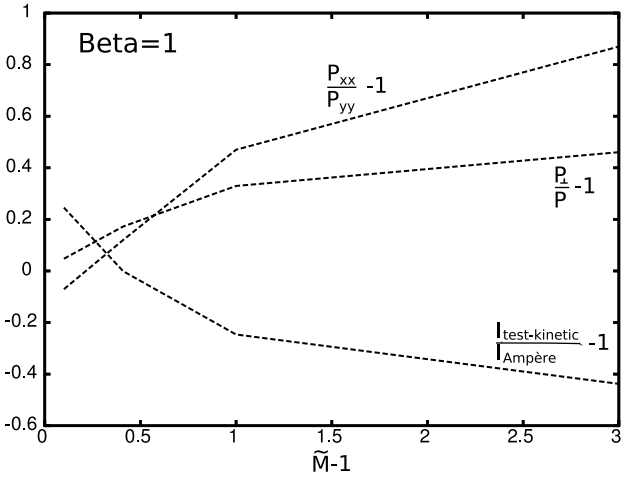



**Figure 8.** Scaling of the spatially averaged pressure anisotropy $P_\perp/P$, $P_{xx}/P_{yy}$ and discrepancy in the depth integrated current density as a function of the Mach number $\tilde{M}$. All ratios are calculated from spatially averaged quantities so as to be uniquely defined in the shocked region. In all cases, the upstream plasma beta is equal to unity.

averaged, depth integrated current density with the corresponding value inferred from Ampère's law. Simulations have been made for $\beta$ and $\tilde{M}$ ranging over the intervals $1/4 < \beta < 4$ and $1.1 < \tilde{M} < 4$. Results are shown in Figs 7 and 8. There is no intent here to extract compelling trends from these plots, particularly in view of the approximate (not fully self-consistent) nature of the approach. It is nonetheless interesting to note that, within our formalism, pressure anisotropy is well behaved over the entire parameter space considered. It is nearly independent of $\beta$, and it is

https://doi.org/10.1017/S0022377808007095 Published online by Cambridge University Press

a weakly increasing function of $\tilde{M}$. Phase bunching, on the other hand, appears to be strongest for low values of $\beta$ or high values of $\tilde{M}$. Under these conditions, the plasma drift velocities are large compared with the thermal velocity, and the bulk distribution of particles tends to closely follow the trajectory of particles for which the distribution function $f$ is maximum. This situation is well illustrated by the example case presented earlier in this section (cf. Figs 1 and 2). Consistency with Ampère's law, on the other hand, is also seen to be the worst at lower and higher values of $\beta$, and the higher values of $\tilde{M}$. Our measure of pressure anisotropy and phase bunching may be indicative of a qualitative dependence of these variables on plasma $\beta$ and $\tilde{M}$. The breakdown of consistency, however, can only be interpreted as an indication of the limits of the macroscopic (ideal MHD) approach used in obtaining the fields. Thus, in modelling a plane perpendicular shock, these results indicate that the Rankine–Hugoniot solution would likely become quantitatively less reliable at low/higher values of $\beta$ ($\beta < 0.5, \beta > 4$) and higher values of the Mach numbers ($\tilde{M} > 2.5$).

## 5. Conclusions

A test-kinetic approach has been used to assess first-order kinetic effects and consistency of solutions obtained in the ideal MHD approximation. The method consists of obtaining a first approximation of the fields using an approximate macroscopic description of the plasma. Applying Liouville's theorem, these fields are then used, together with symplectic particle trajectory integrations backward in time, to determine the distribution function at arbitrary locations in the plasma. For convenience, the distribution function is discretized on an adaptive grid in momentum space, in which cell refinements are based on octree decomposition. The method has been applied to the case of plane perpendicular shocks in collisionless plasmas, for which the solution is obtained by solving standard Rankine–Hugoniot conditions. Despite its relative simplicity, the collisionless plane shock problem is of interest because of the use of the standard Rankine–Hugoniot conditions in many studies of aspects of shock physics in the literature. The approach is capable of reproducing some basic features of kinetic collisionless shocks, such as pressure anisotropy, phase bunching and the presence of periodic structure downstream of the shock interface. The lack of a fully self-consistent treatment, however, prevents this method from reproducing other aspects of shock waves, such as the evolution of waves and instabilities (Wu et al. 1984), and their effects on the evolution of the particle distribution functions (McKean 1996). Modifications have been suggested to improve the macroscopic description of collisionless shocks, while accounting, for example, for pressure anisotropy (Chao et al. 1995; Lin and Lee 1994). Based on the present study, one might add additional corrections associated, for example, with phase bunching and consistency with Ampère's equation. One use of this approach is also to assess the consistency, or lack thereof, in the calculation of the moments of a particle distribution function, obtained from an approximate underlying model and, whence, assess the reliability of the resulting solution. In the example considered here, we have limited our attention to idealized plane perpendicular shocks, for which many detailed kinetic analyses are available, and for which the validity and limitations of the MHD approximation are well understood. The method presented here, however, is directly applicable to more complex

https://doi.org/10.1017/S0022377808007095 Published online by Cambridge University Press

situations, in which plasma and electromagnetic fields are obtained from large three-dimensional MHD codes, and for which a first estimate of kinetic effect together with an assessment of the validity should prove valuable. When working with fields obtained numerically and parametrized on a discrete grid, we note that it would be necessary to use a suitable interpolation method in order to preserve the continuity and smoothness of the interpolated fields. In particular, when interpolating the magnetic field from a grid, care must be taken so as to preserve $\nabla \cdot \mathbf{B} = 0$ (Mackay et al. 2006).

*Acknowledgements*

This work was supported by the Natural Sciences and Engineering Research Council of Canada and by the Canadian Space Agency. Our work made use of the infrastructure and resources of AICT (Academic Information and Communication Technologies) and the University of Alberta.

## References

Ashour-Abdalla, M., El-Alaoui, M., Peroomian, V., Walker, R. J., Raeder, J., Frank, L. A. and Paterson, W. R. 1999 Source distributions of substorm ions observed in the near-Earth magnetotail. *Geophys. Res. Lett.* **26**, 955–958.

Astudillo, H. F., Livi, S., Marsch, E. and Rosenbauer, H. 1996 Evidence for nongyrotropic alpha particle and proton distribution functions: TAUS solar wind measurements. *Geophys. Res. Lett.* **101**, 24 423–24 432.

Burgess, D. and Scholer, M. 2007 Shock front instability associated with reflected ions at the perpendicular shock. *Plasma Phys.* **14**, 012108-1–9.

Candy, J. and Rozmus, W. 1990 A symplectic integration algorithm for separable Hamiltonian functions. *J. Comp. Phys.* **92**, 230–256.

Chao, J. K., Zhang, X. X. and Song, P. 1995 *Geoph. Res. Lett.* **22**, 2409–2412.

Dasgupta, B., Burrows, R., Zank, G. P. and Webb, G. M. 2006 Hydrodynamics of shock waves with reflected particles. I. Rankine–Hugoniot relations and stationary solutions. *Phys. Plasmas* **13**, 082112-1.

Delcourt, D. C. 2002 Particle acceleration by inductive electric fields in the inner magnetosphere. *J. Atmos. Solar-terr. Phys.* **64**, 551–559.

Delcourt, D. C., Grimald, S., Leblanc, F., Berthelier, J.-J., Millilo, A., Mura, A., Orsini, S. and Moore, T. E. 2003 A quantitative model of the planetary $Na^+$ contribution to Mercury's magnetosphere. *Annales Geoph.* **21**, 1723–1736.

Delcourt, D. C., Malova, H. V. and Zelenyi, L. M. 2006 Quasi-adiabaticity in bifurcated current sheets. *Geoph. Res. Lett.* **33**, 06106 doi:10.1029/2005GL025463.

Egedal, J., Fox, W., Belonohy, E. and Porkolab, M. 2004 Kinetic simulation of the VTF magnetic reconnection experiment. *Comput. Phys. Comm.* **164**, 29–33.

Frey, P. J. and George, P. L. 1999 Maillages: applications aux éléments finis. *Hermes Sciences Publicat.*

Gosling, J. T., Asbridge, J. R., Bame, S. J., Paschmann, G. and Sckopke, N. 1978 Solar wind stream interfaces. *Geophys. Res. Lett.* **5**, 957.

Haruki, T. Sakai, J. I. and Saito, S. 2006 Electromagnetic wave emission during collision between a current sheet and a fast magnetosonic shock associated with coronal mass ejections. *Astron. Astrophys.* **455**, 1099–1103.

Hozumi, S. 1997 A phase-space approach to collisionless stellar systems using a particle method. *Astrophys. J.* **487**, 617–624.

Jaeger, E. F. and Speiser, T. W. 1974 Energy and pitch angle distributions for auroral ions using the current sheet acceleration model. *Astrophys. Space Sci.* **28**, 129–144.

https://doi.org/10.1017/S0022377808007095 Published online by Cambridge University Press

Jones, F. C. and Ellison, D. C. 1991 The plasma physics of shock acceleration. *J. Space Sci. Rev.* **58**, 259–346.

Kabin, K. 2000 MHD simulation of magnetospheric interaction of planets and satellites. *PhD Dissertation*, University of Michigan.

Kantrowitz, A. and Petschek, H. E. 1966 *Plasma Physics in Theory and Application.* New York: McGraw-Hill.

Karimabadi, H., Krauss-Varban, D. and Omidi, N. 1995 Temperature anisotropy effects and the generation of anomalous slow shocks. *Geophys. Res. Lett.* **22**, 2689–2692.

Lee, M. A., Shapiro, V. D. and Sagdeev, R. Z. 1996 Pickup ion energization by shock surfing. *J. Geophys. Res.* **101**, 4777–4789.

Lembege, B. and Dawson, J. M. 1987 Self-consistent study of a perpendicular collisionless and nonresistive shock. *Phys. Fluids* **30**, 1767–1788.

Lever, E. L., Quest, K. B. and Shapiro, V. D. 2001 Shock surfing vs. shock drift acceleration. *Geophys. Res. Lett.* **28**, 1367–1370.

Lin, Y. and Lee, L. C. 1994 Structure of reconnection layers in the magnetosphere. *Space Sci. Rev.* **65**, 59–179.

Lyu, L. H. and Kan, J. R. 1986 Shock jump conditions modified by pressure anisotropy and heat flux for Earth's bowshock. *J. Geophys. Res.* **91**, 6771–6775.

Mackay, F., Marchand, R. and Kabin, K. 2006 Divergence-free magnetic field interpolation and charged particle trajectory integration. *J. Geophys. Res.* **111**, A06205, doi:10.1029/2005JA011382.

McKean, M. E., Omidi, N. and Krauss-Varban, D. 1995 Wave and ion evolution downstream of quasi-perpendicular bow shocks. *J. Geophys. Res.* **100**, 3427–3437.

McKean, M. E. 1996 Magnetosheath dynamics downstream of low Mach number shocks. *J. Geophys. Res.* **101**, 20013–20022.

Meziane, K., Mazelle, C., Lin, R. P., LeQueau, D., Larson, D. E., Parks, G. K. and Lepping, R. P. 2001 Three-dimensional observations of gyrating ion distributions far upstream from the Earth's bow shock and their association with low-frequency waves. *J. Geophys. Res.* **106**, 5731–5742.

Moore, T. E., Giles, B. L., Delcour, D. C. and Fok, M.-C. 2000 The plasma sheet source groove. *J. Atmos. Solar-terr. Phys.* **62**, 505–512.

Moore, T. E. et al. 2005 Plasma sheet and (nonstorm) ring current formation from solar and polar wind sources. *J. Geophys. Res.* **110**, A02210, doi:10.1029/2004JA010563.

Othmer, C., Glassmeier, K. H., Motschmann, U., Schule, J. and Frick, Ch. 2000 Three-dimensional simulations of ion thruster beam neutralization. *Phys. Plasmas* **7**, 5242–5251.

Richard, R. L., El.-Alaoui, M., Ashour-Abdalla, M. and Walker, R. J. 2002 Interplanetary magnetic field control of the entry of solar energetic particles into the magnetosphere. *J. Geophys. Res.* **107**, A02210, doi:10.1029/2001JA000099.

Sanderson, J. J. and Uhrig Jr., R. A. 1978 Extended Rankine–Hugoniot relations for collisionless shocks. *J. Geophys. Res.* **83**, 1395–1400.

Sanz-Serna, J. M. 1988 Runge-Kutta schemes for Hamiltonian systems. *BIT Computer Science and Numerical Mathematics* **28**, 877–883.

Schwartz, J. S., Burgess, D. and Moses, J. J. 1996 Low-frequency waves in the Earth's magnetosheath: present status. *Ann. Geophys.* **14**, 1134–1150.

Shimada, M. and Yoshida, H. 1996 Long-term conservation of adiabatic invariants by using symplectic integrators. *Astron. Soc. Japan* **48**, 147–155.

Stuchi, T. J. 2002 Symplectic integrators revisited. *Brazilian J. Phys.* **32**, 958–979.

Suris, Yu. B. 1989 On the canonicity of mappings that can be generated by methods of Runge-Kutta type for integrating systems $\ddot{x} = -\partial U/\partial x$. *Zh. Vychisl. Mat. i Mat. Fiz* **29**, 202–211.

Takeuchi, S. 2005 New particle accelerations by magnetized plasma shock waves. *Phys. Plasmas* **12**, 102901-1–6.

https://doi.org/10.1017/S0022377808007095 Published online by Cambridge University Press

Tanaka, M., Goodrich, C. C., Winske, D. and Papadopoulos, K. 1983 A source of the backstreaming ion beams in the foreshock region. *J. Geophys. Res.* **88**, 3046–3054.

Thomas, V. A. 1989 Dimensionality effects in hybrid simulations of high Mach number collisionless perpendicular shocks. *J. Geophys. Res.* **94**, 12009–12014.

Thomas, V. A. and Winske, D. 1990 Two dimensional hybrid simulation of a curved bow shock. *Geophys. Res. Lett.* **17**, 1247–1250.

Yong, H., Hu, X., Hu, Y., Jiang, Z. and Lu, J. 2006 Rankine-Hugoniot relations of an axial shock in cylindrical non-neutral plasma. *Phys. Plasmas* **13**, 92116-1–5.

Wu, C. S. et al. 1984 Microinstabilities associated with a high Mach number, perpendicular bow shock. *Space Sci. Rev.* **37**, 63–109.

Yoshida, H. 1993 Recent progress in the theory and application of symplectic integrators. *Cel. Mech. Dynam. Astron.* **56**, 27–43.

Zank, G. P., Pauls, H. L., Cairns, I. H. and Webb, G. M. 1996 Interstellar pickup ions and quasi-perpendicular shocks: implications for the termination and interplanetary shocks. *J. Geophys. Res.* **101**, 457–477.

Zank, G. P., Li, G., Florinski, V., Hu, Q, Lario, D. and Smith, C. W. 2006 Particle acceleration at perpendicular shock waves: Model and observations. *J. Geophys. Res.* **111**, A06108, doi:10.1029/2005JA011524.

https://doi.org/10.1017/S0022377808007095 Published online by Cambridge University Press